Journal of Materials Chemistry C

Two Isomeric Perylenothiophene Diimides: Physicochemical Properties and Applications in Organic Semiconducting Devices

Journal:	*Journal of Materials Chemistry C*
Manuscript ID	TC-ART-11-2018-005577.R1
Article Type:	Paper
Date Submitted by the Author:	13-Jan-2019
Complete List of Authors:	Nakano, Masahiro; RIKEN Center for Emergent Matter Science (CEMS), Emergent Molecular Function Research Group Nakano, Kyohei; RIKEN, Center for Emergent Matter Science Tajima, Keisuke; RIKEN Center for Emergent Matter Science (CEMS), Supramolecular Chemistry Division Takimiya, Kazuo; Rikagaku Kenkyujo, Center for Emergent Matter Scienece

Journal Name

ARTICLE

Two Isomeric Perylenothiophene Diimides: Physicochemical Properties and Applications in Organic Semiconducting Devices

Masahiro Nakano,[a*] Kyohei Nakano,[b] Kazuo Takimiya,[a,c*] Keisuke Tajima[b]

Received 00th January 20xx,
Accepted 00th January 20xx

DOI: 10.1039/x0xx00000x

www.rsc.org/

Two thiophene-fused perylene-3,4,9,10-tetracarboxy diimides, peryleno[2,1-*b*]thiophene diimide (PTIa) and peryleno[1,2-*b*]thiophene diimide (PTIb), were synthesized as electron-deficient building units for electronic and optoelectronic materials. Both PTIs have an absorption band in the 480–600 nm range, fluorescence emission with high quantum yield (PTIa: ϕ^{flu} = 0.82 and PTIb: ϕ^{flu} = 0.85) in the 600–700 nm range, and a low-lying LUMO energy level (−3.9 eV). Moreover, the functionalizable α-positions of the fused thiophenes of PTIs allowed us to develop PTI-based π-extended molecules as organic semiconducting materials. Dimerized PTIs (dPTIa and dPTIb) were synthesized for organic field-effect transistors (OFETs), and acceptor-donor-acceptor type triads (IDT-PTIa and IDT-PTIb) were developed as electron-accepting materials for organic photovoltaics (OPVs). The two dPTIs, dPTIa and dPTIb, have different physicochemical properties even though their structural difference is only the direction of the fused thiophenes of the PTI units. The same can be said for the two IDT-PTIs. The PTIa-based materials tend to have higher HOMO energy levels and more bathochromically shifted absorptions than those of the PTIb-counterparts. The differences in the physicochemical properties affected the properties of the organic devices: dPTIa-based OFETs showed ambipolar behaviors, whereas dPTIb-based ones worked as n-channel unipolar OFETs; IDT-PTIa–based OPVs exhibited NIR photo-response up to 880 nm, whereas IDT-PTIb–based ones showed photocurrent generation only up to 800 nm. These results indicate that PTIa and PTIb are an interesting pair of electron-deficeint building units that can tune the electronic structures of resulting organic semiconductors.

Introduction

Over the past two decades, organic π-conjugated molecules have been intensively studied owing to their interesting optical/electronic properties and potential applications in electronic devices.[1,2,3,4] Rylene diimides (RyDIs, Figure 1a), which are well-known π-conjugated systems with excellent photochemical stabilities and strong electron-accepting properties, have received growing attention in the development of organic dyestuffs, pigments, and semiconductors.[5,6,7] Because the physicochemical properties of RyDIs are dependent on the electronic nature of the central rylene cores, the π-extension of the rylene cores is one of the effective ways to tune the absorption/fluorescence and the frontier orbital energy levels of RyDIs for optical and electronic materials. Numerous laterally π-extended RyDIs, particularly lateral-extended naphthalene-1,4,5,8-tetracarboxy diimides (NDIs) and perylene-3,4,9,10-tetracarboxy diimides (PDIs), have been reported as optical materials with visible and/or near-infrared (NIR) photo-responses,[8,9,10] n-type materials for organic field-effect transistors (OFETs),[11,12,13] and electron-accepting materials for organic photovoltaics (OPVs).[14,15,16]

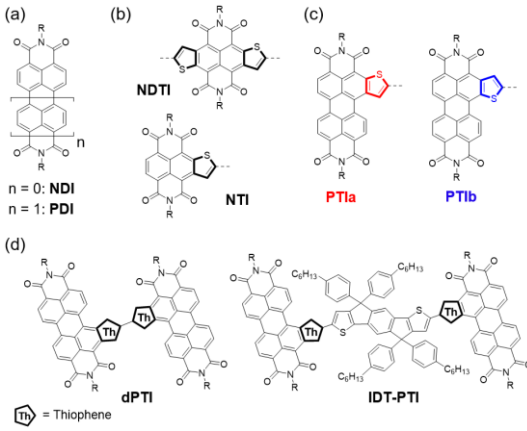

Figure 1. Chemical structures of rylene diimides (a), lateral-extended NDIs with fused thiophenes (b), PTIs (c), and π-extended PTIs (d).

Among the laterally π-extended RyDIs, we have focused on thiophene-fused NDIs (NTI and NDTI, Figure 1b).[17,18,19] Indeed, the fused thiophenes of NTI and NDTI not only alter the physicochemical properties of NDI, but also allow the further development of laterally π-extended materials through the functionalizable α-positions. NTI and NDTI have been adopted as useful building units for π-conjugated molecules with strong

[a] Emergent Molecular Function Research Team, RIKEN Center for Emergent Matter Science (CEMS), 2-1, Hirosawa, Wako, Saitama, 351-0198, Japan.
[b] Emergent Functional Polymers Research Team, RIKEN Center for Emergent Matter Science (CEMS), 2-1, Hirosawa, Wako, Saitama, 351-0198, Japan.
[c] Department of Chemistry, Graduate School of Science, Tohoku University, 6-3, Aoba, Aramaki, Aoba-ku, Sendai, 980-8578, Japan.
*Email - masahiro.nakano@riken.jp
†Electronic Supplementary Information (ESI) available. See DOI: 10.1039/x0xx00000x

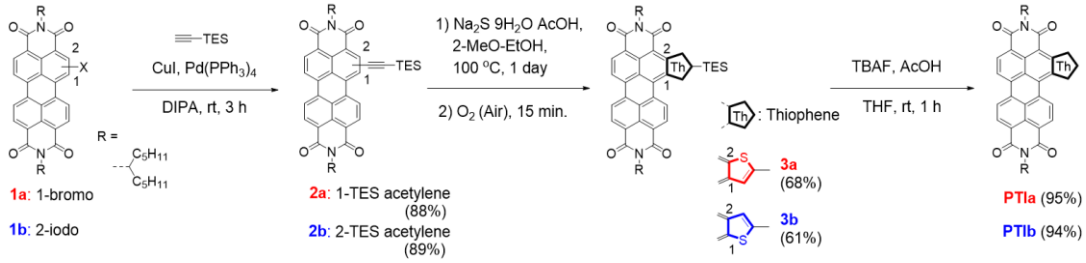

Scheme 1. Synthetic routes of PTIa and PTIb.

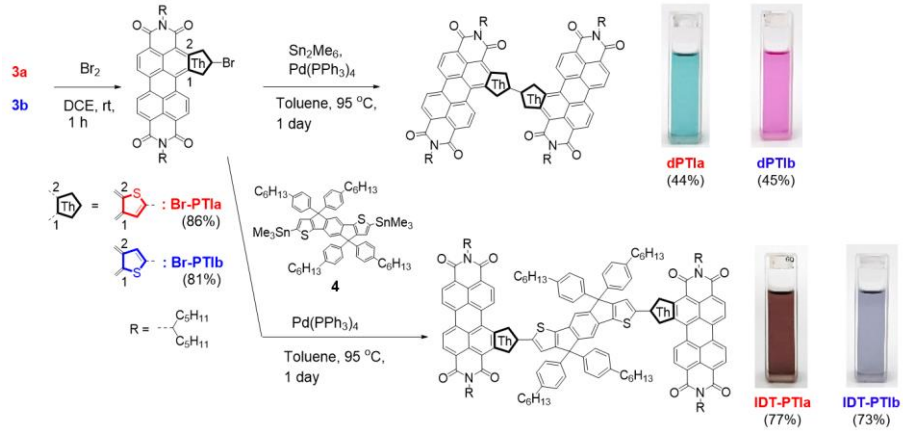

Scheme 2. Synthesis of dPTIs and IDT-PTIs.

electron deficiency, and various NTI- and NDTI-based conjugated molecules and polymers have been developed for n-type OFETs (electron mobility: $\mu_{electron}$ >1 cm^2 V^{-1} s^{-1}),[20] OPVs (power conversion efficiency: PCE >9%),[21] and thermoelectric devices (power factor: PF >14 μW m^{-1} K^{-2}).[22]

On the other hand, the longitudinal π-extension of the rylene cores in RyDIs (i.e., increasing the number of *peri*-condensed naphthalenes in the rylene moiety) can also alter the physicochemical properties.[23,24] For example, *N*,*N*′-dioctyl-NDI shows an absorption in the UV region (280–380 nm, absorption coefficient: ε ~2×10^4 cm^{-1} M^{-1}) and a very weak fluorescence (quantum yield: ϕ^{flu} was lower than the detectable limit by our hands), whereas *N*,*N*′-dioctyl-PDI has an intense absorption in the visible region (450–550 nm, ε ~9×10^4 cm^{-1} M^{-1}) and a strong fluorescence (ϕ^{ful} ~0.95) (Figure S1). Based on the observed intense absorption and high fluorescence quantum yield of *N*,*N*′-dioctyl-PDI, we have expected thiophene-fused PDIs (PTIs, Figure 1c) would be interesting electron-deficient building units for optical and optoelectronic materials. In addition, the large electron-deficient π-skeletons of the PTI units can be advantageous for efficient electron transport in organic electronic devices. Very recently, mono-, di-, and tetra-thiophene–fused PDIs have been reported by several research groups.[25,26,27] Compared to the parent PDI, these thiophene-fused PDIs exhibit absorptions with bathochromic shifts, and tetra-thiophene–fused PDIs show good $\mu_{electron}$s in single-crystal OFETs. These results have encouraged us to study the properties and features of PTIs as building units of π-functional materials.

In this paper, we report the synthesis of mono-thiophene–fused PDIs, peryleno[2,1-*b*]thiophene diimide (PTIa) and peryleno[1,2-*b*]thiophene diimide (PTIb), as electron deficient π-units. Their different direction of the fused thiophen on the PDI skeleton can give the distinct features,[28,29,30] thus, we first elucidate similarities and differences in the electronic structures of the two isomeric PTIs, and then their application to π-extended materials for organic electronic devices are examined: PTI-dimers connected by a coplanar thiophene-thiophene junction (Figure 1d, dPTIa and dPTIb) and acceptor-donor-acceptor triads (Figure 1d, IDT-PTIa and IDT-PTIb) with indaceno[1,2-*b*:5,6-*b*′]dithiophene (IDT).[31,32] The formers are tested as the active material for OFET devices, whereas the latter as the electron accepter in OPV devices combined with an electron donating polymer.

Results and discussion

Synthesis

Scheme 1 shows the synthesis of PTIa and PTIb. We first prepared ethynylated PDIs with 1-pentylhexyl groups at the imide moieties (**2a** and **2b**) by Sonogashira cross-coupling reaction of the corresponding halogenated PDIs (**1a** and **1b**, Scheme S1) with triethylsilyl (TES) acetylene. Then, **2a** and **2b** were converted into the PTI structures (**3a** and **3b**) by a sodium sulfide–promoted thiophene annulation reaction (Figure S2)[33,34] in isolated yields of 68 and 61%, respectively. The subsequent desilylation with tetrabutylammonium fluoride gave PTIa and PTIb as maroon solids, which were fully characterized by spectroscopic methods, including IR, ^{1}H NMR, ^{13}C NMR, and high-resolution MS (See Experimental section).

The TES group of **3a** and **3b** were readily converted into bromine in high isolated yields (Br-PTIa: 86% and Br-PTIb: 81%, Scheme 2). Palladium-catalyzed reactions of the brominated PTI with hexamethylditin gave dimerized PTIs

(dPTIa and dPTIb). IDT-PTIa and IDT-PTIb were synthesized by the Stille cross-coupling reaction of corresponding Br-PTIs with 2,7-bis(trimethylstannyl)-IDT (**4**). All the compounds were isolated as stable solids and fully characterized. It is noteworthy that the colours of isomeric dPTIs and IDT-PTIs are not the same, even though the structural difference is only the direction of the fused thiophenes; dPTIa: emerald green, dPTIb: pink, IDT-PTIa: dark brown, and IDT-PTIb: purple in chloroform solution, respectively (vide infra).

Physicochemical properties

Figure 2a and 2b show the absorption and fluorescence spectra of PTIa, PTIb, and PDI. Table 1 summarizes their physicochemical properties. PTIa and PTIb show bathochromic shifts in absorption and fluorescence in chloroform solution relative to parent PDI. These bathochromic shifts in PTIs are attributed to the π-extension of PDI by thiophene condensation. The high fluorescence quantum yields of PTIs (PTIa: ϕ^{flu} = 0.82 and PTIb: ϕ^{flu} = 0.85) indicate that the strong fluorescence of PDI is not impaired by the thiophene condensation.

The electrochemical behaviour of PTIs is similar to that of PDI (Figure S3a); the cyclic voltammograms of PTIs show two separate reversible reduction waves and one irreversible oxidation wave (from −1.9 V to +1.2 V, vs. Fc/Fc^+). The frontier orbital energy levels of PTIa and PTIb were estimated from the onset values of the oxidation and reduction waves. The estimated HOMO and LUMO energy levels (E_{HOMO}s and E_{LUMO}s) of PTIa and PTIb are the same (E_{HOMO} = −5.7 eV and E_{LUMO} = −3.9 eV).

The absorption spectra and cyclic voltammograms of dPTIs and IDT-PTIs are depicted in Figure 2cd and S3b. In contrast to the similarity in the physicochemical properties of PTIa and PTIb, dPTIa and dPTIb have different absorption and E_{HOMO}s (Table 1). dPTIa has more bathochromically shifted absorption (λ_{edge}^{abs} ~719 nm) and higher E_{HOMO} (−5.6 eV) than those of dPTIb (λ_{edge}^{abs} ~695 nm, E_{HOMO} = −5.8 eV), and both of dPTIs have similar E_{LUMO}s (−4.1 eV). Similar tendencies in the absorption and frontier orbital energy levels are also observed in IDT-PTIs. Both of IDT-PTIs exhibit absorption in the visible to the NIR region, and IDT-PTIa show bathochromic shifts in the absorption (λ_{edge}^{abs} ~857 nm) compared to IDT-PTIb (λ_{edge}^{abs} ~801 nm). The E_{HOMO} of IDT-PTIa (−5.3 eV) is higher than that of IDT-PTIb (−5.4 eV).

To clarify the difference in electronic properties between the π-extended PTIas and the PTIb-counterparts, we studied their frontier orbitals from the results of the density functional theory (DFT) calculations with 6-31G* basis set (Figure 3). The calculated E_{HOMO}s of PTIa-based molecules are higher than those of the corresponding PTIb-based ones, and their E_{LUMO}s are similar. These trends are similar to the experimental results. The difference of E_{HOMO}s of dPTIa and dPTIb can be understood by considering how the molecular orbitals of the two PTI-units in dPTIs interact with each other. dPTIa shows well-delocalized HOMO on the whole molecular structure through the thiophene-thiophene junction. This suggests that the orbital mixing of the HOMOs of the two PTIa-units is effective, which can give the higher E_{HOMO} of dPTIa than that of parent PTIa.[35] On the other hand, the HOMO of dPTIb is localized on the two PTIb-units.

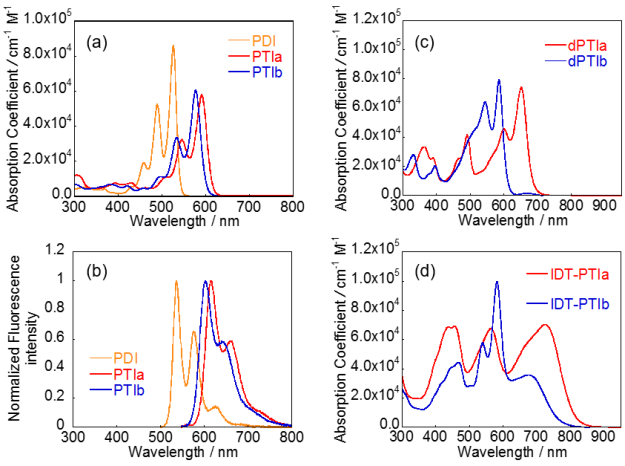

Figure 2. Absorption spectra and fluorescence spectra of PTIs and PDI (a, b). Absorption spectra of dPTIs and IDT-PTIs (c, d).

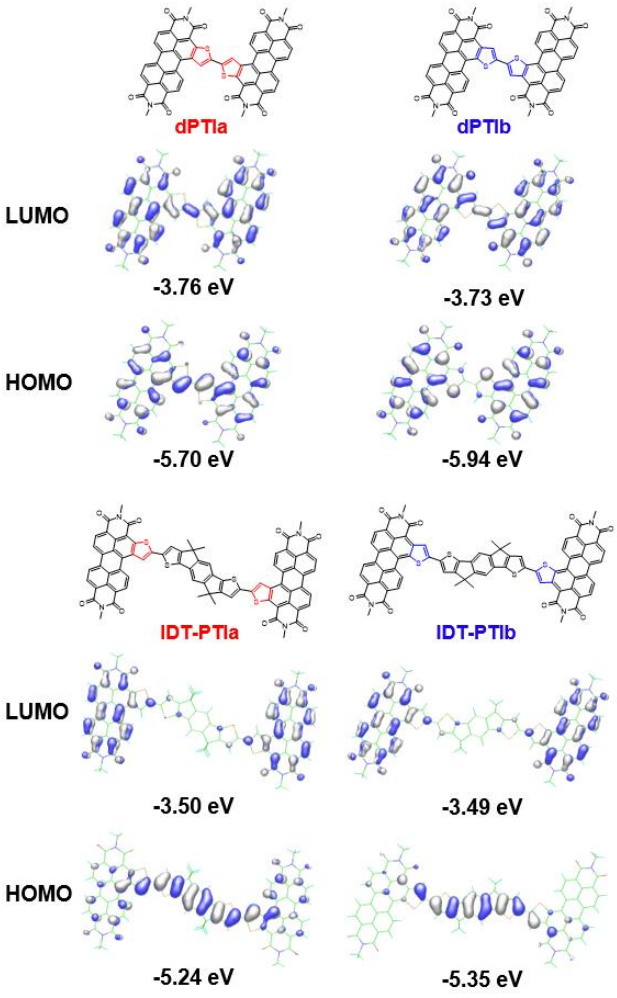

Figure 3. DFT-calculated HOMO and LUMO of dPTIs and IDT-PTIs.

Table 1. Physicochemical properties of PDI, PTIs, NTI, and π-extended PTIs

Compounds	λ_{edge}^{abs} / nm[a]	E_g / eV[b]	λ_{max}^{flu} / nm[c]	ϕ^{flu} [d]	E_{red}^{onset} / V [e]	E_{LUMO} / eV[f]	E_{oxi}^{onset} / V [e]	E_{HOMO} / eV[g]
PDI	551	2.32	535	0.96	−1.04	−3.8	1.09	−5.9
PTIa	624	2.05	621	0.82	−0.94	−3.9	0.92	−5.7
PTIb	612	2.09	612	0.85	−0.95	−3.9	0.94	−5.7
dPTIa	719	1.78	–	–	−0.74	−4.1	0.77	−5.6
dPTIb	695	1.84	–	–	−0.75	−4.1	1.04	−5.8
IDT-PTIa	857	1.49	–	–	−0.86	−3.9	0.48	−5.3
IDT-PTIb	801	1.60	–	–	−0.89	−3.9	0.58	−5.4

[a]UV-visible absorption spectra measured in chloroform solution (ca. 10^{-5} M) at room temperature. [b]Calculated from the λ_{edge}^{abs}, E_g = 1240/λ_{edge}^{abs}. [c]Fluorescence spectra measured in chloroform solution (ca. 10^{-6} M). [d]Absolute quantum yield. [e]Against ferrocene/ferrocenium couple. [f]E_{LUMO} = –4.8 – E_{red}^{onset} (eV). [g]E_{HOMO} = –(E_{oxi}^{onset} + 4.8) (eV).

This implies that the orbital interaction of the PTIb-units is weaker compared with that of PTIa-units in dPTIa though the dihedral angle of the α,α´-linked thiophenes of dPTIb is similar to that of dPTIa (<5°, Figure S6a). As a consequence, the E_{HOMO} of dPTIb is lower than that of dPTIa. In the case of IDT-PTIs, the dihedral angles the α,α´-linked thiophenes in the DFT-optimized structures of IDT-PTIs are also similar (Figure S6b), however, the HOMO of IDT-PTIa is more delocalized than that of IDT-PTIb, which indicates that the orbital mixing of PTIa- and IDT-units is more effective than that of PTIb- and IDT-units. This can explain the higher E_{HOMO} of IDT-PTIa than that of IDT-PTIb. These difference in the HOMO of π-extended PTIas and corresponding PTIbs would be originated from the different HOMO distribution of PTIa and PTIb (Figure S7): the HOMO coefficient at the α-carbon atom of PTIa is larger than that of PTIb (PTIa: 0.166 and PTIb: 0.063), which can give more effective orbital mixing of HOMOs of PTIa and substituted π-units than that of PTIb and adjacent units. These results suggest that we can use PTIa- and PTIb-units to control the physicochemical properties of PTI-based materials: PTIa is effective for the molecular design of materials with a narrow HOMO–LUMO energy gap, whereas PTIb is useful for the molecules with lower E_{HOMO}s than the corresponding PTIa-based ones.

OFET and OPV properties

As characterized by cyclic voltammetry, dPTIs exhibit sufficient E_{LUMO}s (−4.1 eV) for electron-transportation in OFET devices under ambient conditions.[36] OFET devices with a bottom-gate/top-contact configuration were fabricated with spin-coated thin films of dPTIa and dPTIb on Si/SiO_2 substrates treated with octyldodecyltrichlorosilane (ODTS).

Figure 4 shows the transfer and output characteristics of the transistors, and Table S3 summarizes their properties. The dPTIa- and dPTIb-based devices show transistor characteristics for n-channel operation (V_d = +60 V) under ambient conditions, thereby suggesting that PTIs are promising building units for air-stable n-type OFET materials. The dPTIa-based transistors exhibit ambipolar characteristics (on/off ratio: I_{on}/I_{off} ~10^2) owing to the low-lying E_{LUMO} and the high-lying E_{HOMO} (−5.6 eV). By contrast, the lower E_{HOMO} of dPTIb (−5.8 eV) does not allow the injection of hole carriers, resulting in typical n-type characteristics (I_{on}/I_{off} ~10^5).

The maximum $\mu_{electron}$s of dPTIa- and dPTIb-based devices were 1.0×10^{-2} and 8.4×10^{-3} cm^2 V^{-1} s^{-1}, respectively. Atomic force microscopy (AFM) images of the devices based on dPTIa and dPTIb are similar (Figure S8ab), which can explain their similar electron mobilities. Improved $\mu_{electron}$s were obtained after thermal annealing at 200 °C (dPTIa: $\mu_{electron}$ ~9.2×10^{-2} cm^2 V^{-1} s^{-1} and dPTIb: $\mu_{electron}$ ~4.3×10^{-2} cm^2 V^{-1} s^{-1}). In AFM images of the annealed devices, crystalline grains with submicrometer were observed more clearly compared with those of non-annealed devices (Figure S8cd). Besides, we evaluated the molecular orientation of dPTIs in thin films with and without thermal annealing by XRD measurements. The as-cast films of dPTIa and dPTIb show only one diffraction peak (dPTIa: d = 19.7 Å, dPTIb: d = 19.9 Å) in the out-of-plane XRD patterns (Figure S10ab). After thermal annealing (200 °C), the thin films of dPTIs show not only diffraction peaks in the out-of-plane XRD patterns (dPTIa: d = 21.9 Å, dPTIb: d = 22.4 Å) but also broad peaks, which are attributed to the π-stacking ordering, in the in-plane patterns (Figure S10cd, dPTIa: d = 3.5 Å, dPTIb: d = 3.5 Å). These results indicate that dPTIs showed perpendicular orientation of their π-plane to the substrate in the annealed thin-films (Figure S10), which can lead to improved mobilities in the annealed OFET devices.

We also fabricated IDT-PTIa– and IDT-PTIb–based OFETs, and the molecular orientation of IDT-PTIs in the thin films were evaluated. Both of the devices based on the as-cast films of IDT-PTIa and IDT-PTIb did not show any clear transistor characteristics. This can be explained by the low-crystalline nature of IDT-PTIa and IDT-PTIb; Neither of the as-cast films of IDT-PTIs showed any peaks in the XRD patterns (Figure S11). After thermal annealing (200 °C), weak diffraction peaks were observed in the out-of-plane (IDT-PTIa: d = 21.2 Å, IDT-

PTIb: d = 21.2 Å) and the in-plane (IDT-PTIa: d = 20.8 Å, IDT-PTIb: d = 20.8 Å) XRD patterns. Although annealed OFETs based on IDT-PTIa and IDT-PTIb did not work, we measured the electron mobilities of the annealed films by SCLC method (Figure S13 and Table S1). The SCLC mobilities of IDT-PTIa and IDT-PTIb in the thin films are also similar, which can be understand from their similar molecular orientation manner.

On the other hand, the broad absorption in the visible to the NIR region implies usefulness of IDT-PTIs in OPV devices with NIR photo-responses. We fabricated OPV devices with an inverted configuration, where PBDB-T, a representative state-of-the-art donor material,[37,38,39] was combined with IDT-PTIs. Figure 5 shows the *J-V* characteristics and the external quantum efficiency (EQE) spectra of IDT-PTIa– and IDT-PTIb–based OPVs. The OPVs have similar PCEs of 3.8% (IDT-PTIa:PBDB-T) and 3.5% (IDT-PTIb:PBDB-T). Due to the bathochromic shift in the absorption of IDT-PTIa relative to that of IDT-PTIb (Figure S4), the OPV devices based on IDT-PTIa have an EQE spectrum with an NIR photo-response up to 880 nm.

Thermal annealing improved the OPV performances (200 °C, IDT-PTIa:PBDB-T: PCE = 5.1% and IDT-PTIb:PBDB-T: PCE = 4.9%), particularly the short-circuit current density (J_{SC}) and the fill factor (FF). The similar AFM images of the OPV devices with and without annealing implies that there are not significant morphological differences in the annealed and non-annealed devices (Figure S9). On the other hand, out-of-plane and in-plane XRD measurements indicated that the crystalline nature of the blended films of IDT-PTIa:PBDB-T and IDT-PTIb:PBDB-T was improved after the thermal annealing (Figure S12). The enhanced crystallinity of the blended films may explain the improvement of J_{SC} and FF values of the annealed devices. The well-distributed carrier delocalization in the ordered active materials can give improved J_{SC} and FF owing to the enhancement of the dissociation of the charge-transfer excitons.[40,41] Similar device behaviours upon thermal annealing were also observed in reported OPVs based on electron-accepting materials with molecular structures close to that of IDT-PTIs.[21,42]

The d-spacing values estimated from the out-of-plane and in-plane XRD patterns of the annealed blend-films are d = 20.4 Å and d = 20.7 Å, respectively. These d-spacing values are the same as those of the pure films of PBDB-T and are different from those of IDT-PTIs, indicating that the IDT-PTIs do not form an ordered structure in annealed blend films. The poor molecular orientation of IDT-PTIs in the active layers can limit the resulting PCE values. However, the moderate PCE values of IDT-PTI-based OPVs suggest that PTI-units are promising for electron accepting materials with NIR absorbing nature.

Conclusions

In summary, mono-thiophene-fused PDIs, PTIa and PTIb, were synthesized as building units for organic electronic and optoelectronic materials with strong electron deficiencies. Both show bathochromic shift in the absorption/fluorescence spectra and downward shift of the E_{LUMO}s compared with those of PDI. We also synthesized dPTIs (dPTIa and dPTIb) for n-type OFET

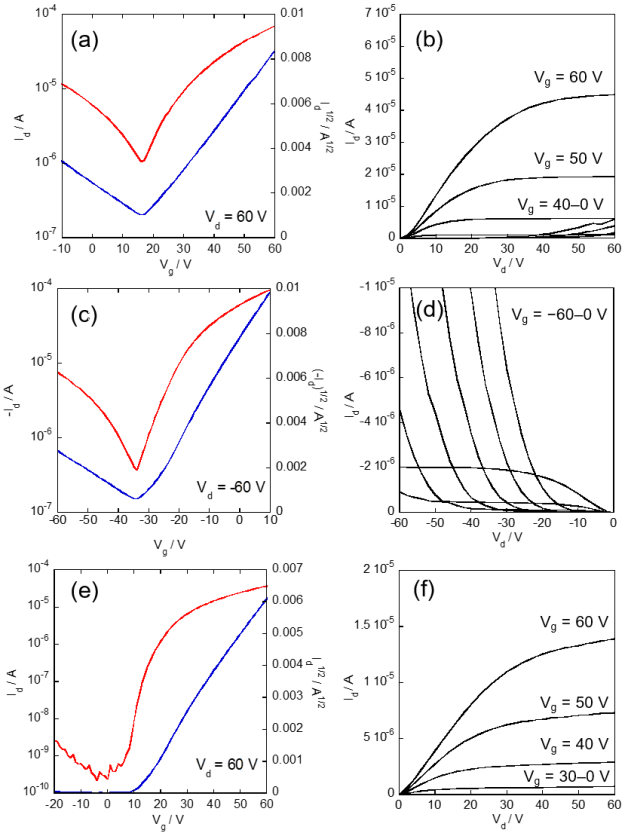

Figure 4. Transfer and Output curves of bottom-gate-top-contact type OFETs based on dPTIa (a,b,c,d) and dPTIb (e,f). W/L = 1500/40. All the devices were characterized under ambient conditions.

materials and IDT-PTIs (IDT-PTIa and IDT-PTIb) as electron-accepting materials for OPVs. The physicochemical properties of PTIa and PTIb are similar, but the results of DFT calculations indicated that the HOMO coefficient at the α-carbon atoms of PTIs are differ. As a consequence, both dPTIs and IDT-PTIs

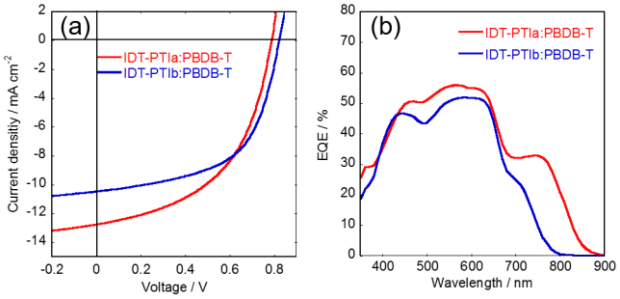

Figure 5. *J-V* characteristics (a) and EQE spectra (a) of the OPV devices based on IDT-PTIa:PBDB-T and IDT-PTIb:PBDB-T.

have different physicochemical properties depending on the type of PTI-unit in the molecular structures; dPTIa and IDT-PTIa showed higher E_{HOMO}s and more bathochromic shifts in absorption than the corresponding PTIb-based derivatives. The different physicochemical properties affected the properties of the organic devices based on dPTIs and IDT-PTIs: dPTIa-based

OFETs demonstrated ambipolar behaviours, whereas dPTIb-based OFETs worked as n-channel OFETs. IDT-PTIa–based OPVs exhibited NIR photo-response up to 880 nm, which is bathochromically shifted relative to that of IDT-PTIb–based devices (–800 nm). These results suggest that PTIa- and PTIb-units can tune the physicochemical properties and resulting behaviour in organic devices of PTI-based molecules. The further design and synthesis of PTI-based π-conjugated materials and studies of their possible utilization in organic electronic and optoelectronic devices are underway in our laboratory.

Experimental

General

All chemicals and solvents are of reagent grade unless otherwise indicated. Toluene were purified with a standard procedure prior to use. 2,7-bis(trimethylstannyl)-4,4,9,9-tetrakis(4-hexylphenyl)-*s*-indaceno[1,2-*b*:5,6-*b*´]dithiophene, [43] and PBDB-T[33] were synthesized according to the reported procedures. All reaction was conducted under argon atmosphere. Melting points were uncorrected. Nuclear magnetic resonance spectra were obtained in deuterated chloroform ($CDCl_3$) or deuterated 1,1,2,2-tetrachloroethane (TCE-d_2); chemical shifts (δ) are reported in parts per million. IR spectra were recorded using a KBr pellet.

Synthesis

***N,N´*-Bis(1-pentylhexyl)-1-(triethylsilylethynyl)-perylene-3,4,9,10-tetracarboxydiimide (2a)**

A mixture of **1a** (2.0 g, 2.57 mmol), triethylsilylacetylene (1.22 mL, 6.8 mmol), bis(triphenylphosphine)palladium(II) dichloride (600 mg, 0.85 mmol), and copper iodide (52 mg, 0.27 mmol) in diisopropylamine (70 mL) was stirred under room temperature for 1 day. After evaporation of the solvent, the residue was purified by column chromatography on silica gel eluted with dichloromethane/hexane (1:2, v/v) to give **2a** as a red solid (1.89 g, 88%): ^{1}H NMR (400 MHz, TCE-d_2): δ 10.53 (d, *J* = 8.0 Hz, 1H), 8.85 (s, 1H), 8.75 (d, *J* = 8.0 Hz, 1H), 8.74–8.68 (m, 4H), 5.26–5.17 (m, 2H), 2.44–2.22 (m, 4H), 2.04–1.90 (m, 4H), 1.49–1.32 (m, 24H), 1.27 (t, *J* = 8.0 Hz, 9H), 0.98–0.91 (m, 18H); ^{13}C NMR (100 MHz, TCE-d_2): 164.2, 164.0, 163.6, 163.4, 139.2, 134.82, 134.75, 134.5, 134.2, 131.4, 131.1, 131.0, 129.4, 128.9, 127.54, 127.48, 127.0, 124.4, 124.2, 123.8, 123.6, 123.1, 122.9, 122.8, 120.4, 107.6, 106.2, 55.2, 32.7, 31.8, 26.8, 22.6, 13.9, 7.7, 4.8; IR (KBr) ν = 1699, 1661 cm^{-1} (C=O); MP: 217.6–218.4 °C; HRMS (APCI) m/z calcd for $C_{54}H_{68}N_2O_4Si$: $[M]^+$ 837.5027. Found: 837.5022.

***N,N´*-Bis(1-pentylhexyl)-2-(triethylsilylethynyl)-perylene-3,4,9,10-tetracarboxydiimide (2b)**

A similar procedure to the synthesis of **2a** with **1b** afforded the title compound as a red solid in 89% isolated yield: ^{1}H NMR (400 MHz, $CDCl_3$): δ 8.70 (d, *J* = 8.0 Hz, 1H), 8.69 (d, *J* = 8.0 Hz, 1H), 8.68 (d, *J* = 8.0 Hz, 1H) 8.64 (s, 1H), 8.62 (d, *J* = 8.0 Hz, 1H), 8.61 (d, *J* = 8.0 Hz, 1H), 8.60 (d, *J* = 8.0 Hz, 1H), 5.23–5.15 (m, 2H), 2.31–2.20 (m, 4H), 1.93–1.84 (m, 4H), 1.39–1.23 (m, 24H), 1.20 (t, *J* = 8.0 Hz, 9H), 0.89–0.83 (m, 18H); ^{13}C NMR (100 MHz, TCE-d_2): 164.1, 163.5, 162.1, 161.8, 134.7, 134.2, 134.0, 133.3, 131.8, 131.7, 131.5, 131.4, 130.3, 129.7, 129.6, 129.4, 127.5, 126.7, 126.0, 124.9, 124.3, 124.1, 123.1, 123.0, 105.9, 105.7, 55.2, 55.1, 32.7, 31.8, 26.74, 26.69, 22.5, 13.9, 7.47, 7.42, 4.91; IR (KBr) ν = 1701, 1680 cm^{-1} (C=O); MP: 150.4–151.1 °C; HRMS (APCI) m/z calcd for $C_{54}H_{68}N_2O_4Si$: $[M]^+$ 837.5027. Found: 837.5023.

***N,N´*-Bis(1-pentylhexyl)-2-(triethylsilyl)-peryleno[2,1-*b*]thiophene-6,7,12,13-tetracarboxydiimide (3a)**

$Na_2S{\cdot}9H_2O$ (770 mg, 3.20 mmol) was added to a stirred suspension of **2a** (1.48 g, 1.77 mmol) in 2-methoxyethanol (162 mL) and acetic acid (1.7 mL) at 100 °C. After stirred at the same temperature for 12 h, the mixture was stirred again at room temperature for 15 min. under atmospheric conditions. Then, the mixture was diluted with water and the resulting precipitate was collected by filtration and washed with methanol. After drying, the crude product was purified by column chromatography (SiO_2, dichloromethane/hexane = 1/2) to give **3a** as a maroon solid (0.99 g, 68%): ^{1}H NMR (400 MHz, $CDCl_3$): δ 8.82 (d, *J* = 8.0 Hz, 1H), 8.80 (d, *J* = 8.0 Hz, 1H), 8.75 (d, *J* = 8.0 Hz, 1H), 8.72 (d, *J* = 8.0 Hz, 1H), 8.68 (d, *J* = 8.0 Hz, 1H), 8.65 (d, *J* = 8.0 Hz, 1H), 8.44 (s, 1H), 5.53–5.18 (m, 4H), 2.37–2.34 (m, 4H), 2.00–1.84 (m, 4H), 1.45–1.23 (m, 24H), 1.16–0.99 (m, 15H), 0.85 (t, *J* = 6.8 Hz, 6H), 0.83 (t, *J* = 6.8 Hz, 6H); ^{13}C NMR (100 MHz, TCE-d_2): 164.4, 164.2, 164.1, 164.0, 152.4, 149.2, 140.1, 136.0, 134.94, 134.85, 131.26, 131.17, 130.34, 129.67, 129.58, 128.61, 127.5, 126.6, 125.2, 123.9, 123.6, 123.3, 123.1, 122.5, 120.6, 116.3, 55.4, 55.2, 32.77, 31.9, 26.82, 26.76, 22.5, 13.88, 13.87, 7.4, 4.7; IR (KBr) ν = 1699.6, 1647.2 cm^{-1} (C=O); MP: 132.8–134.0 °C; HRMS (APCI) m/z calcd for $C_{54}H_{66}N_2O_4SSi$: $[M]^+$ 869.4747. Found: 869.4748.

***N,N´*-Bis(1-pentylhexyl)-2-(triethylsilyl)-peryleno[1,2-*b*]thiophene-4,5,10,11-tetracarboxydiimide (3b)**

A similar procedure to the synthesis of **3a** with **2b** afforded the title compound as a maroon solid in 61% isolated yield: ^{1}H NMR (400 MHz, $CDCl_3$): δ 9.28 (d, *J* = 8.0 Hz, 1H), 9.28 (s, 1H), 8.83 (d, *J* = 8.0 Hz, 1H) , 8.82 (d, *J* = 8.0 Hz, 1H), 8.74–7.69 (m, 3H), 5.32–5.17 (m, 2H), 2.35–2.26 (m, 4H), 2.08–1.83 (m, 4H), 1.38–1.24 (m, 24H), 1.18–1.04 (m, 15H); ^{13}C NMR (100 MHz, TCE-d_2): 164.5, 164.2, 164.1, 164.0, 149.9, 144.7, 143.1, 135.1, 134.8, 134.1, 133.4, 131.5, 131.1, 131.0, 129.5, 129.4, 128.1, 127.6, 127.4, 124.6, 124.4, 123.8, 123.5, 122.9, 122.8, 116.9, 55.2, 55.1, 32.8, 32.7, 31.9, 31.8, 26.8, 26.7, 22.5, 13.9, 7.4, 4.7; IR (KBr) ν = 1691.6, 1653.6 cm^{-1} (C=O); MP: 139.2–140.2 °C; HRMS (APCI) m/z calcd for $C_{54}H_{66}N_2O_4SSi$: $[M]^+$ 869.4747. Found: 869.4746.

***N,N´*-Bis(1-pentylhexyl)-peryleno[2,1-*b*]thiophene-6,7,12,13-tetracarboxydiimide (PTIa)**

3a (100 mg, 0.13 mmol) was dissolved in THF (10 mL) and acetic acid (1.0 mL), and then, tetra-*n*-butylammmonium fluoride (1.0 M in THF, 1.3 mL) was added to the solution at 0 °C. After stirred for 1 h at room temperature, the solution was diluted with methanol (100 mL). The resulting precipitate was collected by filtration and washed with methanol and purified by

column chromatography (SiO_2, dichloromethane/hexane = 1/2) to afford PTIa as a maroon solid. (82 mg, 95%): ^{1}H NMR (400 MHz, TCE-d_2): δ 8.86 (d, *J* = 8.0 Hz, 1H), 8.84 (s, *J* = 8.0 Hz, 1H), 8.78 (d, *J* = 8.0 Hz, 1H), 8.76 (d, *J* = 8.0 Hz, 1H), 8.70 (d, *J* = 8.0 Hz, 1H), 8.68 (d, *J* = 8.0 Hz, 1H), 8.42 (d, *J* = 6.8 Hz, 1H), 8.11 (d, *J* = 6.8 Hz, 1H), 5.33 (tt, *J* = 8.4 Hz, 6.0 Hz, 1H), 5.25 (tt, *J* = 8.4 Hz, 6.0 Hz, 1H), 2.43–2.77 (m, 4H), 2.09–1.96 (m, 4H), 1.54–1.32 (m, 24H), 0.94 (t, *J* = 6.8 Hz, 6H), 0.93 (t, *J* = 6.8 Hz, 6H); ^{13}C NMR (100 MHz, , TCE-d_2): 164.4, 164.2, 164.0, 163.9, 145.8, 138.6, 137.2, 135.7, 134.9, 134.7, 131.3, 131.2, 131.0, 130.3, 129.6, 129.5, 127.4, 126.7, 125.2, 124.0, 123.7, 123.3, 123.2, 122.6, 116.7, 99.9, 55.4, 55.2, 32.8, 31.9, 26.8, 22.5, 13.9; IR (KBr) ν = 1691.6, 1647.2 cm^{-1} (C=O); MP: 217.7–218.5 °C HRMS (APCI) m/z calcd for $C_{48}H_{54}N_2O_4S$: $[M]^+$ 755.3883. Found: 755.3883.

N,N´-Bis(1-pentylhexyl)-peryleno[1,2-*b*]thiophene-4,5,10,11-tetracarboxydiimide (PTIb)

A similar procedure to the synthesis of PTIa with **3b** afforded the title compound as a maroon solid in 94% isolated yield: ^{1}H NMR (400 MHz, TCE-d_2): δ 9.19 (d, *J* = 8.0 Hz, 1H), 9.18 (d, *J* = 8.0 Hz, 1H), 8.82 (d, *J* = 8.0 Hz, 1H) , 8.80 (s, *J* = 8.0 Hz, 1H), 8.73 (d, *J* = 8.0 Hz, 1H), 8.68 (s, *J* = 6.8 Hz, 1H), 8.03 (d, *J* = 6.8 Hz, 1H), 5.28 (tt, *J* = 8.4 Hz, 6.0 Hz, 1H), 5.21 (tt, *J* = 8.4 Hz, 6.0 Hz, 1H), 2.36–2.28 (m, 4H), 2.01–1.82 (m, 4H), 1.54–1.32 (m, 24H), 0.90 (t, *J* = 6.8 Hz, 6H), 0.89 (t, *J* = 6.8 Hz, 6H); ^{13}C NMR (100 MHz, TCE-d_2): 164.5, 164.2, 164.0, 164.0, 143.6, 139.3, 134.8, 134.7, 134.0, 131.5, 131.3, 130.1, 129.5, 128.1, 127.3, 126.7, 126.4, 124.8, 124.2, 123.9, 123.7, 123.1, 122.7, 117.4, 99.9, 55.3, 55.2, 32.83, 32.76, 31.91, 31.88, 26.9, 26.8, 22.6, 14.0; IR (KBr) ν = 1693.5, 1654.9 cm^{-1} (C=O); MP: 232.9–234.5 °C; HRMS (APCI) m/z calcd for $C_{48}H_{54}N_2O_4S$: $[M]^+$ 755.3883. Found: 755.3887.

N,N´-Bis(1-pentylhexyl)-2-bromoperyleno[2,1-*b*]thiophene-6,7,12,13-tetracarboxydiimide (Br-PTIa)

Bromine (2.15 g, 13.4 mmol) was added to a stirred suspension of **3a** (315 mg, 0.363 mmol) in dichloroethane (21 mL) at room temperature and the mixture was stirring at the same temperature. After the disappearance of the starting material (TLC monitoring, usually 30 min.), the mixture was quenched with diluted $NaHSO_3$ aqueous solution (30 mL) and extracted with dichloromethane (50 mL). Then, the solvent was evaporated and the residue was purified by column chromatography on silica gel eluted with dichloromethane/hexane (1:3, v/v) to give Br-PTIa as a dark red solid (260 mg, 86%): ^{1}H NMR (400 MHz, $CDCl_3$): δ 8.80 (d, *J* = 8.0 Hz, 1H), 8.74 (s, 2H), 8.73 (d, *J* = 8.0 Hz, 1H), 8.67 (d, *J* = 8.0 Hz, 1H), 8.65 (d, *J* = 8.0 Hz, 1H), 8.36 (s, 1H), 5.29–5.17 (m, 2H), 2.35–2.23 (m, 4H), 1.97–1.84 (m, 4H), 1.43–1.19 (m, 24H), 0.96 (t, *J* = 6.8 Hz, 6H), 0.95 (t, *J* = 6.8 Hz, 6H); ^{13}C NMR (100 MHz, TCE-d_2): 164.3, 164.0, 163.9, 163.7, 146.9, 137.9, 135.1, 134.8, 131.4, 131.3, 131.2, 129.4, 128.8, 128.7, 128.1, 127.2, 126.4, 125.7, 125.2, 124.1, 123.9, 123.2, 123.0, 122.7, 115.7, 55.6, 55.2, 32.8, 32.7, 31.9, 31.8, 26.8, 22.5, 13.9; IR (KBr) ν = 1690.5, 1654.8 cm^{-1} (C=O); MP: 201.7–203.4 °C; HRMS (EI) m/z calcd for $C_{48}H_{53}BrN_2O_4S$: $[M]^+$ 833.2988. Found: 833.2993.

N,N´-Bis(1-pentylhexyl)-2-bromoperyleno[1,2-*b*]thiophene-4,5,10,11-tetracarboxydiimide (Br-PTIb)

A similar procedure to the synthesis of Br-PTIb with **3b** afforded the title compound as a dark red solid in 81% isolated yield: ^{1}H NMR (400 MHz, TCE-d_2): δ 9.28 (s, 1H), 8.86 (d, *J* = 8.0 Hz, 1H), 8.81 (d, *J* = 8.0 Hz, 1H), 8.80 (d, *J* = 8.0 Hz, 1H), 8.68 (d, *J* = 8.0 Hz, 1H), 8.66 (d, *J* = 8.0 Hz, 1H), 5.27 (tt, *J* = 8.4 Hz, 6.0 Hz, 2H), 2.42–2.32 (m, 4H), 2.12–2.01 (m, 4H), 1.48–1.36 (m, 24H), 0.94 (t, *J* = 6.8 Hz, 12H); ^{13}C NMR (100 MHz, TCE-d_2): 164.1, 164.0, 163.70, 163.66, 149.4, 143.1, 140.0, 136.7, 134.1, 134.0, 133.8, 132.1, 131.3, 131.2, 129.4, 128.7, 128.1, 127.0, 124.9, 124.5, 124.0, 123.9, 123.1, 122.83, 122.77, 116.1, 55.4, 55.3, 32.79, 32.75, 31.9 26.9, 26.8, 22.5, 13.9; IR (KBr) ν = 1690.4, 1655.0 cm^{-1} (C=O); MP: 267.8–269.8 °C; HRMS (EI) m/z calcd for $C_{48}H_{53}BrN_2O_4S$: $[M]^+$ 833.2988. Found: 833.2999.

[2,2′]Bi[peryleno[2,1-*b*]thienyl]-*N,N′,N′′,N′′′*-tetrakis(1-pentylhexyl)-6,6′,7,7′,12,12′,13,13′-tetraimide (dPTIa)

Hexamethylditin (16 mg, 0.049mmol) was added into a solution of Br-PTIa (84 mg, 0.101 mmol), and $Pd(PPh_3)_4$, (5.4 mg, 0.0045 mmol, 18 mg) in 3 mL of toluene. The solution was heated at 95 °C for 18 h. After cooling to room temperature, the mixture was evaporated under vacuum, and the residue was purified by column chromatography (SiO_2, toluene/chloroform = 3/1) to afford dPTIa as a dark green solid (33 mg, 44%); ^{1}H NMR (400 MHz, $CDCl_3$): 8.93 (s, 4H), 8.83 (d, *J* = 8.0 Hz, 2H), 8.81 (s, 2H), 8.78 (d, *J* = 8.0 Hz, 2H), 8.72 (d, *J* = 8.0 Hz, 2H), 8.69 (d, *J* = 8.0 Hz, 2H), 5.35 (tt, *J* = 8.4 Hz, 6.0 Hz, 2H), 5.27 (tt, *J* = 8.4 Hz, 6.0 Hz, 2H), 2.44–2.27 (m, 8H), 2.08–1.89 (m, 8H), 1.43–1.25 (m, 48H), 0.89 (t, *J* = 6.8 Hz, 12H), 0.85 (t, *J* = 6.8 Hz, 12H); ^{13}C NMR (100 MHz, TCE-d_2): 164.4, 164.1, 163.84, 163.75, 146.2, 146.1, 138.9, 135.2, 134.9, 134.4, 131.7, 131.6, 131.3, 130.6, 129.6, 128.7, 127.3, 126.1, 125.7, 124.2, 124.1, 123.7, 123.3, 123.0, 122.7, 116.3, 55.7, 55.3, 32.7, 31.9, 26.9, 26.8, 22.6, 13.9; MP: >350 °C; IR (KBr): ν = 1690.5, 1643.3 cm^{-1} (C=O); HRMS (EI) m/z calcd for $C_{48}H_{54}N_2O_4S_2$: $[M]^+$ 1507.7566. Found: 1507.7580.

[2,2′]Bi[peryleno[1,2-b]thienyl]-*N,N′,N′′,N′′′*-tetrakis(1-pentylhexyl)-4,4′,5,5′,10,10′,11,11′-tetraimide (dPTIb)

A similar procedure to the synthesis of dPTIa with Br-PTIb afforded the title compound as a dark red solid in 45% isolated yield: ^{1}H NMR (400 MHz, TCE-d_2): 9.78 (s, 2H), 9.31 (d, *J* = 8.0 Hz, 2H), 9.00 (d, *J* = 8.0 Hz, 2H), 8.88 (d, *J* = 8.0 Hz, 2H), 8.82 (d, *J* = 8.0 Hz, 2H), 8.77 (d, *J* = 8.0 Hz, 2H), 8.76 (d, *J* = 8.0 Hz, 2H), 5.40 (tt, *J* = 8.8 Hz, 6.0 Hz, 2H), 5.28 (tt, *J* = 8.4 Hz, 6.0 Hz, 2H), 2.49–2.31 (m, 8H), 2.17–1.99 (m, 8H), 1.43–1.35 (m, 48H), 0.96 (t, *J* = 6.8 Hz, 12H), 0.95 (t, *J* = 6.8 Hz, 12H); ^{13}C NMR (100 MHz, TCE-d_2):164.4, 164.1, 163.5, 163.4, 143.7, 143.0, 138.9, 135.6, 134.2, 133.9, 133.5, 131.3, 131.1, 129.4, 128.4, 127.1, 127.0, 125.9, 125.2, 124.1, 124.00, 123.96, 122.9, 122.8, 117.6, 99.9, 55.7, 55.3, 32.9, 32.8, 32.0, 31.9, 27.1, 26.8, 22.7, 22.6, 14.0, 13.9; IR (KBr) ν = 1695.5, 1651.1 cm^{-1} (C=O); MP: >350 °C; HRMS (EI) m/z calcd for $C_{48}H_{54}N_2O_4S_2$: $[M]^+$ 1507.7566. Found: 1507.7556.

***N,N´,N´´,N´´´*-Tetrakis(1-pentylhexyl)-2,7-bis(peryleno[2,1-*b*]thiophen-2-yl)-4,4,9,9-tetrakis(4-hexylphenyl)-*s*-indaceno[1,2-*b*:5,6-*b*´]dithiophene-6´,6´´,7´,7´´,12´,12´´,13´,13´´-octacarboxytetraimide (IDT-PTIa)**

A mixture of 2,7-bis(trimethylstannyl)-4,4,9,9-tetrakis(4-hexylphenyl)-*s*-indaceno[1,2-*b*:5,6-*b*´]dithiophene (100 mg, 0.0811 mmol), Br-PTIa (140 mg, 0.168 mmol), $Pd(PPh_3)_4$ (14 mg, 0.012 mmol), copper(I) iodide (2.5 mg, 0.0130 mmol), and toluene (3.5 mL) was heated to 95 °C. After cooling to room temperature, the mixture was evaporated under vacuum, and the residue was purified by column chromatography (SiO_2, dichloromethane/hexane = 1/1) to afford IDT-PTIa as a black solid (150 mg, 77%); ^{1}H NMR (400 MHz, $CDCl_3$): δ 8.81 (d, *J* = 8.0 Hz, 2H), 8.79 (d, *J* = 8.0 Hz, 2H), 8.75 (d, *J* = 8.0 Hz, 2H), 8.73 (d, *J* = 8.0 Hz, 2H), 8.66 (d, *J* = 8.0 Hz, 2H), 8.64 (d, *J* = 8.0 Hz, 2H), 7.57 (s, 2H), 7.56 (s, 2H), 7.24 (d, *J* = 8.4 Hz, 8H), 7.14 (d, *J* = 8.4 Hz, 8H), 5.31–5.20 (m, 4H), 2.61 (t, *J* = 8.4 Hz, 8H), 2.38–2.37 (m, 8H), 2.00–1.84 (m, 8H), 1.64 (quin, *J* = 8.4 Hz, 8H), 1.43–1.21 (m, 72H), 0.89–0.82(m, 36H); ^{13}C NMR (100 MHz, TCE-d_2):164.5, 164.2, 164.03, 163.95, 158.4, 148.2, 146.1, 144.3, 142.1, 141.1, 139.7, 139.5, 135.8, 135.7, 134.8, 134.6, 131.4, 131.3, 130.8, 129.7, 128.74, 128.68, 128.1, 127.9, 127.8, 126.8, 125.7, 124.0, 123.9, 123.4, 123.0, 122.6, 118.2, 117.5, 116.0, 99.9, 63.8, 55.5, 55.1, 35.6, 32.78, 32.75, 31.9, 31.8, 31.0, 29.7, 29.2, 26.80, 26.77, 22.53, 13.9; IR (KBr) ν = 1691.6, 1643.3 cm^{-1} (C=O); MP: >350 °C; HRMS (FD) m/z calcd for $C_{160}H_{178}N_4O_8S_4$: $[M]^+$ 2411.25275. Found: 2411.24715.

***N,N´,N´´,N´´´*-Tetrakis(1-pentylhexyl)-2,7-bis(peryleno[1,2-*b*]thiophen-2-yl)-4,4,9,9-tetrakis(4-hexylphenyl)-*s*-indaceno[1,2-*b*:5,6-*b*´]dithiophene-4´,4´´,5´,5´´,10´,10´´,11´,11´´-octacarboxytetraimide (IDT-PTIb)**

A similar procedure to the synthesis of IDT-PTIa with Br-PTIb afforded the title compound as a purple solid in 73% isolated yield: ^{1}H NMR (400 MHz, $CDCl_3$): δ 9.27 (s, 2H), 9.12 (d, *J* = 8.0 Hz, 2H), 8.83 (d, *J* = 8.0 Hz, 2H), 8.80 (d, *J* = 8.0 Hz, 2H), 8.74 (d, *J* = 8.0 Hz, 2H), 8.69 (d, *J* = 8.0 Hz, 2H), 8.68 (d, *J* = 8.0 Hz, 2H), 7.63 (s, 2H), 7.56 (s, 2H), 7.27 (d, *J* = 8.4 Hz, 8H) , 7.16 (d, *J* = 8.4 Hz, 8H), 5.32–5.20 (m, 4H), 2.62 (t, *J* = 8.4 Hz, 8H), 2.36–2.24 (m, 8H), 1.97–1.84 (m, 8H), 1.65 (quin, *J* = 8.4 Hz, 8H), 1.43–1.21 (m, 72H), 0.89–0.82 (m, 36H); ^{13}C NMR (100 MHz, TCE-d_2): 164.4, 164.2, 164.0, 163.9, 158.3, 154.9, 145.6, 144.9, 142.1, 141.1, 138.9, 138.8, 135.7, 134.8, 134.7, 133.8, 131.4, 131.2, 129.5, 129.1, 128.8, 128.7, 128.2, 127.3, 127.0, 124.8, 124.1, 123.9, 123.8, 123.7, 122.9, 12.4, 120.4, 118.3, 116.0, 99.9, 63.8, 55.3, 55.2, 35.7, 32.9, 32.8, 31.9, 31.8, 31.0, 29.2, 26.9, 26.8, 22.6, 13.9; IR (KBr) ν = 1699.5, 1651.0 cm^{-1} (C=O); MP: >350 °C; HRMS (FD) m/z calcd for $C_{160}H_{178}N_4O_8S_4$: $[M]^+$ 2411.25275. Found: 2411.25975.

Measurement of physicochemical properties

UV-vis absorption spectra were measured on a Shimadzu UV-3600 spectrometer in chloroform solution (concentration: 10^{-5}–10^{-4} M). Fluorescence spectra were obtained with absolute PL quantum yield spectrometer C11347 (Hamamatsu Photonics) in chloroform solution (concentration: 10^{-6}–10^{-5} M). Cyclic voltammograms (CVs) were recorded on an ALS Electrochemical Analyzer Model 612D in benzonitrile containing tetrabutylammonium hexafluorophosphate (Bu_4NPF_6, 0.1 M) as supporting electrolyte at a scan rate of 100 mV s^{-1}. Counter and working electrodes were made of Pt. All the potentials were calibrated with the standard ferrocene/ferrocenium redox couple (Fc/Fc^+: $E_{1/2}$ = +0.47 V).

Theoretical calculations

Geometry optimizations and normal mode calculations of isolated molecules were performed at the B3LYP/6-31G* level using the Gaussian 09 program package.[44] All the model compounds have methyl groups at their imide moieties to simplify the calculations.

Conflicts of interest

There are no conflicts to declare.

Acknowledgements

We acknowledge the financial support from JSPS KAKENHI Grant Numbers 15H02196 and 16K05900, and the Strategic Promotion of Innovative Research and Development from JST. HRMSs were carried out at the Molecular Structure Characterization Unit, RIKEN Center for Sustainable Resource Science (CSRS). DFT calculations using Gaussian 09 were performed by using the RIKEN Integrated Cluster of Clusters (RICC).

Notes and references

[1] Y. Shirota, *Chem. Rev.*, 2000, **10**, 1–25.

[2] M. D. Watson, A. Fechtenkötter, K. Müllen, *Chem. Rev.*, 2001, **101**, 1267−1300.

[3] M. Gsänger, D. Bialas, L. Huang, M. Stolte, F. Würthner, *Adv. Mater.*, 2016, **28**, 3615−2645.

[4] Z. Sun, Q. Ye, C. Chi, J. Wu, *Chem. Soc. Rev.*, 2012, **41**, 7857−7889.

[5] C. R. Newman, C. D. Frisbie, D. A. da S. Filho, J.-L. Brédas, P. C. Ewbank, K. R. Mann, *Chem. Mater.*, 2004, **16**, 4436−4451.

[6] S. V. Bhosale, C. H. Jani, S. J. Langford, *Chem Soc. Rev.*, 2008, 37, 331−342.

[7] F. Würthner, M. Stolte, *Chem. Commun.*, 2011, 47, 5109−5115.

[8] F. Würthner, S. Ahmed, C. Thalacker, T. Debaerdemaeker, *Angew. Chem. Eur. J.*, 2002, **8**, 4742−4750.

[9] Y. Li, L. Xu, T. Liu, Y. Yu, H. Liu, Y. Li, D. Zhu, *Org. Lett.*, 2011, **13**, 5692−5695.

[10] M. Kojima, A. Tamoto, N. Aratani, H. Yamada, *Chem. Commun.*, 2017, **53**, 5698−5701.

[11] X. Zhan, A. Facchetti, S. Barlow, T. J. Marks, M. A. Ratner, M. E. Wasielewki, S. R. Marder, *Adv. Mater.*, 2011, **23**, 268−284.

[12] X. Gao, C.-a. Di, Y. Hu, X. Yang, H. Fan, F. Zhang, Y. Liu, H. Li, D. Zhu, *J. Am. Chem. Soc.*, 2010, **132**, 3697–3699.

[13] H. Yan, Z. Chen, Y. Zheng, C. Newman, J. R. Quinn, F. Dotz, M. Kastler, A. Facchetti, *Nature*, 2009, **457**, 679–686.

[14] F. Fernández-Lázaro, N. Zink-Lorre, A. Sastre-Santos, *J. Mater. Chem. A*, 2016, **4**, 9336–9346.

[15] J. Liu, S. Chen, D. Qian, B. Gautam, G. Yang, J. Zhao, J. Bergqvist, F. Zhang, W. Ma, H. Ade, O. Inganäs, K. Gundogdu, F. Gao, H. Yan, H., *Nat. Energy*, 2016, **1**, 16089.

[16] D. Srivani, A. Gupta, S. V. Bhosale, A. L. Puyad, W. Xiang, J. Li, R. A. Evans, S. V. Bhosale, *Chem. Commun.*, 2017, **53**, 7080–7083.

[17] Y. Fukutomi, M. Nakano, J.-Y. Hu, I. Osaka, K. Takimiya, *J. Am. Chem. Soc*., 2013, 135, 11445–11448.

[18] W. Chen, M. Nakano, J.-H. Kim, K. Takimiya, Q. Zhang, *J. Mater. Chem. C*, 2016, **4**, 8879−8883.

[19] K. Takimiya, M. Nakano, *Bull. Chem. Soc. Jpn.*, 2017, **29**, 256−264.

[20] S. Kumagai, M. Nakano, K. Takimiya, J. Takeya, *Org. Electron.*, in Press, DOI: 10.1016/j.orgel.2018.06.029.

[21] J. Hamonnet, M. Nakano, K. Nakano, H. Sugino, K. Takimiya, K. Tajima, *Chem. Mater.*, 2017, **29**, 9618−9622.

[22] Y. Wang, M. Nakano, T. Michinobu, Y. Kiyota, T. Mori, K. Takimiya, *Macromolecules*, 2017, **50**, 657−864.

[23] L. Chen, C. Li, K. Müllen, *J. Mater. Chem. C*, 2014, **2**, 1938–1956.

[24] H. Langhals, D. Zgela, R. Lüling, *J. Org. Chem.*, 2015, **80**, 12146–12150.

[25] C. Zeng, C. Xiao, X. Feng, L. Zhang, W. Jiang, Z. Wang, *Angew. Chem. Int. Ed.*, 2018, **57**, 10933−10937.

[26] During preparation of this manuscript, synthesis of peryleno[1,2-*b*]thiophene diimide derivative which has very similar molecular structure to one of the our target compounds was reported: J. Wu, D. He, Y. Wang, F. Su, Z. Guo, J. Lin, H.-J. Zhang, *Org. Lett*, 2018, 20, 6117–6120.

[27] C. Zeng, D. Meng, W. Jiang, Z. Wang, *Org. Lett.*, 2018, **20**, 6606–6609.

[28] S.-W. Cheng, D.-Y Chiou, Y.-Y Lai, R.-H. Yu, C.-H. Lee, Y.-J. Cheng, *Org. Lett.*, 2013, **15**, 5338−5341.

[29] C. Zhang, Y. Zang, E. Gann, C. R. McNeill, X. Zhu, C.-an Di, D. Zhu, *J. Am. Chem. Soc.*, 2014, **136**, 16176−16184.

[30] Y.-L. Chen, J.-Y. Hsu, F.-Y. Lin, Y.-Y. Lai, H.-C. Chou, Y.-J., Cheng, *J. Org. Chem.*, 2016, **81**, 2534−2542.

[31] C. B. Nielsen, S. Holliday, H.-Y. Chen, S. J. Cryer, I. McCulloch, *Acc. Chem. Res.*, 2015, **48**, 2803–2812.

[32] N. Liang, W. Jiang, J. Hou, Z. Wang, *Mater. Chem. Front.*, 2017, **1**, 1291–1303.

[33] M. S. Shvarsberg, I. D. Ivanchikova, *ARKIVOC*, 2003, **13**, 87−100.

[34] M. Nakano, K. Takimiya, *Chem. Mater.*, 2017, **29**, 256−264.

[35] K. Takmiya, I. Osaka, M. Nakano, *Chem. Mater.*, 2014, **26**, 587−593.

[36] Z. Wang, C. Kim, A. Facchetti, T. J. Marks, *J. Am. Chem. Soc.*, 2007, **129**, 15259–15278.

[37] Poly[(2,6-{4,8-bis[5-(2-ethylhexyl)thiophen-2-yl]benzo[1,2-*b*:4,5-*b*´]dithiophene})-*alt*-{5,5-[1´,3´-di(thiophen-2-yl)-5´,7´-bis(2-

ethylhexyl)benzo[1′,2′-*c*:4′,5′-*c*′]dithiophene-4′,8′-dione]}] (PBDB-T).

[38] D.Qian, L. Ye, M. Zhang, Y. Liang, L. Li, Y. Huang, X. Guo, S. Zhang, Z. Tan, J. Hou, *Macromolecules*, 2012, **45**, 9611–9697.

[39] W. Zhao, D. Qian, S. Zhang, S. Li. O. Inganäs, F. Gao, J. Hou, *Adv. Mater*., 2016, **28**, 4734–4749.

[40] A. Zusan, K. Vandewal, B. Allendorf, N. H. Hansen, J. Pflaum, A. Salleo, V. Dyakonov, C. Deibel, *Adv. Energy Mater.*, 2014, **4**, 1400922.

[41] B. Bernarso, D. Cheyns, B. Verreet, R. D. Schaller, B. P. Rand, N. C. Giebink, *Nat. Commun.*, 2014, **5**, 3245.

[42] Z. Li, D. Yang, T. Zhang, J. Zhang, X. Zhao, X. Yang, *Small*, 2018, **14**, 1704491.

[43] W. Wen, L. Ying, B. B. Y. Hsu, Y. Zhang, T.-Q. Nguyen, G. C. Bazan, *Chem. Commun.*, 2013, **49**, 7192–7194.

[44] Gaussian 09, Revision D.01, Frisch, M. J.; Trucks, G. W.; Schlegel, H. B.; Scuseria, G. E.; Robb, M. A.; Cheeseman, J. R.; Scalmani, G.; Barone, V.; Mennucci, B.; Petersson, G. A.; Nakatsuji, H.; Caricato, M.; Li, X.; Hratchian, H. P.; Izmaylov, A. F.; Bloino, J.; Zheng, G.; Sonnenberg, J. L.; Hada, M.; Ehara, M.; Toyota, K.; Fukuda, R.; Hasegawa, J.; Ishida, M.; Nakajima, T.; Honda, Y.; Kitao, O.; Nakai, H.; Vreven, T.; Montgomery, J. A., Jr.; Peralta, J. E.; Ogliaro, F.; Bearpark, M.; Heyd, J. J.; Brothers, E.; Kudin, K. N.; Staroverov, V. N.; Kobayashi, R.; Normand, J.; Raghavachari, K.; Rendell, A.; Burant, J. C.; Iyengar, S. S.; Tomasi, J.; Cossi, M.; Rega, N.; Millam, J. M.; Klene, M.; Knox, J. E.; Cross, J. B.; Bakken, V.; Adamo, C.; Jaramillo, J.; Gomperts, R.; Stratmann, R. E.; Yazyev, O.; Austin, A. J.; Cammi, R.; Pomelli, C.; Ochterski, J. W.; Martin, R. L.; Morokuma, K.; Zakrzewski, V. G.; Voth, G. A.; Salvador, P.; Dannenberg, J. J.; Dapprich, S.; Daniels, A. D.; Farkas, Ö.; Foresman, J. B.; Ortiz, J. V.; Cioslowski, J.; Fox, D. J. Gaussian, Inc., Wallingford CT, **2009**.

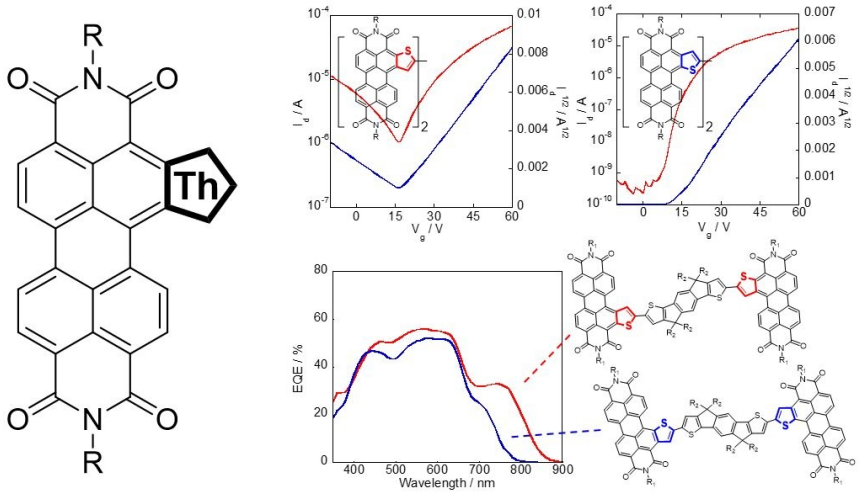

314x156mm (96 x 96 DPI)